5-2001

Overview of Acousto-optic Bistability, Chaos, and Logical Applications

Monish Ranjan Chatterjee
University of Dayton, mchatterjee1@udayton.edu

Erol Sonmez
State University of New York at Binghamton

An overview of acousto-optic bistability, chaos, and logical applications

Monish R. Chatterjee and Erol Sonmez

Department of Electrical Engineering, Watson School, Binghamton University, State University of New York, Binghamton, New York 13902-6000, U.S.A.

ABSTRACT

An overview is presented of the key results in the field of acousto-optic bistability in the past two decades. It is shown that the basic acousto-optic bistable device may be described as a nonlinear dynamical system which satisfies a quadratic map. Thereafter, details are presented of several analytical methods, computer modeling approaches, including the SPICE circuit modeling technique, and experiments that have been used to understand the phenomenon. Extensions to logical and digital applications are also discussed.

Keywords: bistability, chaos, quadratic maps, iteration maps, Bragg cells, hysteresis, optical flip-flops, nonlinear feedback, nonlinear modeling, optical logic

1. INTRODUCTION

In the past two decades, there has been much interest in nonlinear optical devices that exhibit hysteresis, differential gain, and hard limits of the optical output versus input power characteristics [1-8]. It is known that acousto-optic (A-O) devices with feedback gain exhibit bistability characteristics [1,3]. In an acousto-optic device operating in Bragg domain the amplitudes of the two diffracted beams at the output of the Bragg cell are related through a set of coupled differential equations. If the first order diffracted light is detected, amplified and fed back into the acoustic driver, making the acoustic energy a function of diffracted light intensity, the resulting hybrid device exhibits optical bistability with respect to at least three parameters, viz., the acoustic driver bias, the feedback gain, and the incident optical amplitude. One prerequisite for bistability is the presence of a time delay in the feedback path. This is generally provided directly through the photodetector conversion process; in some cases, delay can be separately introduced, as through optical delay lines, such as sections of fibers or transmission lines. The basic hybrid device as well as the standard A-O Bragg cell may also be modified to realize optical flip-flops and other logic devices for possible digital optical applications. In section 2 of this paper, we review the analytical methods previously developed by various research groups, including quadratic maps, trace diagrams, dynamical and bifurcation/chaotic analyses, Fortran programming of two and four-order diffraction, and an early equivalent electrical circuit model of the hybrid feedback system due to Chrostowski *et al.* in 1983 [4]. The concept of using nonlinear SPICE modeling to simulate the bistable device, which was first introduced in by Chatterjee and Huang in 1992 [5] is discussed in some detail in section 3. The development of a set-reset flip-flop using a dual-input device is described in section 4. Other logical devices, such as NOT, AND and OR gates, which incorporate grating control via sound cell phase delay parameter in open-loop Bragg cells are presented with simulations in section 5. Section 6 concludes this paper.

2. THE HYBRID A-O BISTABLE DEVICE: ANALYTICAL METHODS

In this section we discuss some of the analytical approaches previously used for the study of acousto-optic bistability. We consider the case of the hybrid acousto-optic Bragg cell with nonlinear feedback and discuss hysteresis, bistability, multistability, and chaos. Let a beam of amplitude E_{inc} be incident at the Bragg angle. The diffracted light consists of two fields: E_0 (the zeroth order, which is undiffracted) and E_1 (the first order). These fields appear at the output of the Bragg cell at z=L (or equivalently ξ=z/L=1). Incident light can come in two different ways so that we either get an upshifted diffraction or a downshifted diffraction. These cases are illustrated in Fig. 1(a) and 1(b).

Acousto-Optics and Applications, Bogumil B. J. Linde, Anna Sikorska, Editors,
Proceedings of SPIE Vol. 4514 (2001) © 2001 SPIE · 0277-786X/01/$15.00

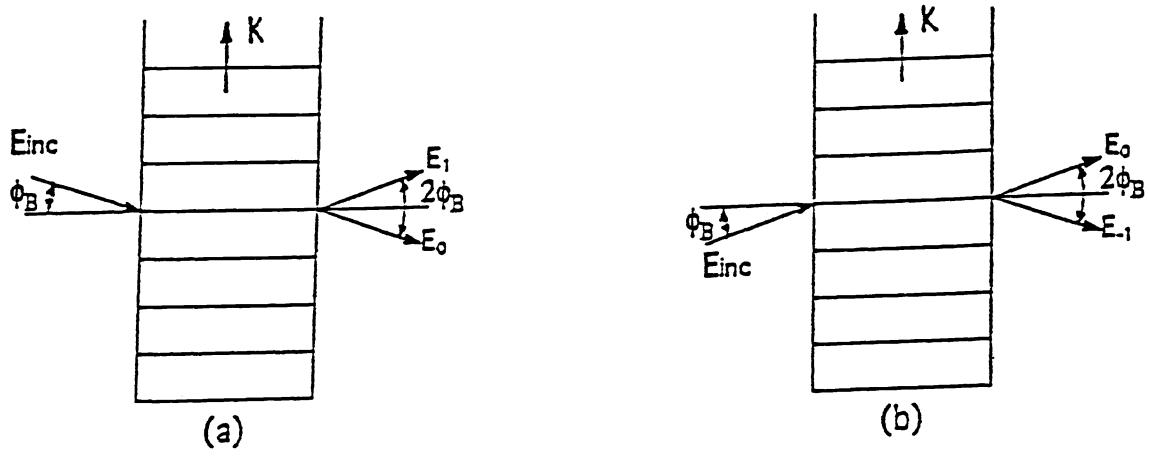

Fig. 1. Acousto-optic device operating in the Bragg regime: (a) upshifted Bragg diffraction, (b) downshifted Bragg diffraction (after [5]).

To determine the diffracted outputs we use the well-known coupled differential equations for the two Bragg orders. Considering upshifted diffraction, the coupled differential equations for E_0 and E_1 within the Bragg cell are given (in terms of the normalized longitudinal distance ξ (= z/L) where L is the so-called interaction width) by [9]

$$\frac{dE_0}{d\xi} = -j\frac{\hat{\alpha}}{2}E_1, \tag{1a}$$

$$\frac{dE_1}{d\xi} = -j\frac{\hat{\alpha}}{2}E_0. \tag{1b}$$

Equations (1a) and (1b) are solved to give

$$E_0(\xi) = A\cos\left(\frac{\hat{\alpha}}{2}\xi\right) + B\sin\left(\frac{\hat{\alpha}}{2}\xi\right), \tag{2a}$$

$$E_1(\xi) = C\cos\left(\frac{\hat{\alpha}}{2}\xi\right) + D\sin\left(\frac{\hat{\alpha}}{2}\xi\right). \tag{2b}$$

With the initial conditions $E_0(0) = E_{inc}$, $E_1(0) = 0$, the solutions for the field inside the Bragg cell may be obtained as

$$E_0(\xi) = E_{inc}\cos\left(\frac{\hat{\alpha}}{2}\xi\right), \tag{3a}$$

$$E_1(\xi) = -jE_{inc}\sin\left(\frac{\hat{\alpha}}{2}\xi\right). \tag{3b}$$

At the output of the Bragg cell (z=l or ξ=1) we have

$$E_0 = E_{inc} \cos\left(\frac{\hat{\alpha}}{2}\right) \quad , \tag{3c}$$

$$E_1 = -jE_{inc} \sin\left(\frac{\hat{\alpha}}{2}\right) \quad , \tag{3d}$$

The above fields may be expressed in intensity form as

$$I_1 = I_{inc} \sin^2\left(\frac{\hat{\alpha}}{2}\right) \quad , \tag{4a}$$

$$I_0 = I_{inc} \cos^2\left(\frac{\hat{\alpha}}{2}\right) \quad , \tag{4b}$$

where $I_o=|E_o|^2$, $I_1=|E_1|^2$, $I_{inc}=|E_{inc}|^2$, and $\hat{\alpha}$ is the total phase delay.

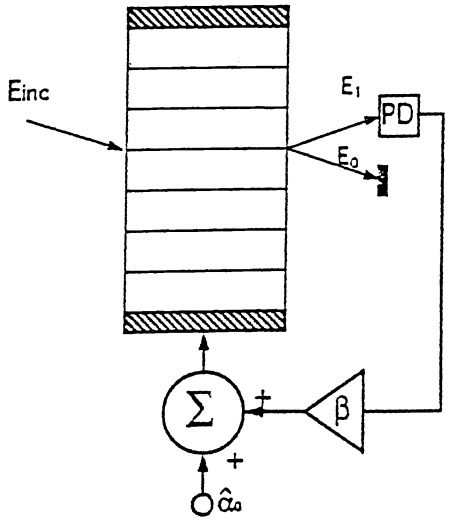

Fig. 2. Hybrid bistable device (after [5]).

Fig. 2 shows a hybrid bistable device based on Bragg diffraction [1,2,8]. An incident field E_{inc} at z=0 generates two fields E_0 and E_1 at z=L. The first-order diffracted field E_1 is detected and fed back into the generator making the acoustic energy a function of the diffracted light intensity. Total phase delay $\hat{\alpha}$ may be expressed as

$$\hat{\alpha} = \hat{\alpha}_o + \beta |E_1|^2, \tag{5}$$

where β is the effective feedback gain, $\hat{\alpha}_0$ is the external bias to the source driver.

The steady state behavior of the device is given by the simultaneous solution of Eqs.(4a) and (5). Note that the intensity on the LHS of Eq.(4), or the amplitude on the LHS of Eq.(3), recurs after a time delay suffered during feedback via the field-dependent $\hat{\alpha}$ parameter (Eq.(5)). This time delay is crucial to bistability and chaos in this dynamical system. Further details are presented in section that follows. There are three modes of operation each leading to a hysteresis curve for the output intensity: (a) varying the input intensity, (b) varying the gain in the feedback path, and (c) varying the bias voltage $\hat{\alpha}_0$. Fig. 3 shows the graphical solutions of eqs.(1a) and (5) for three modes of operation.

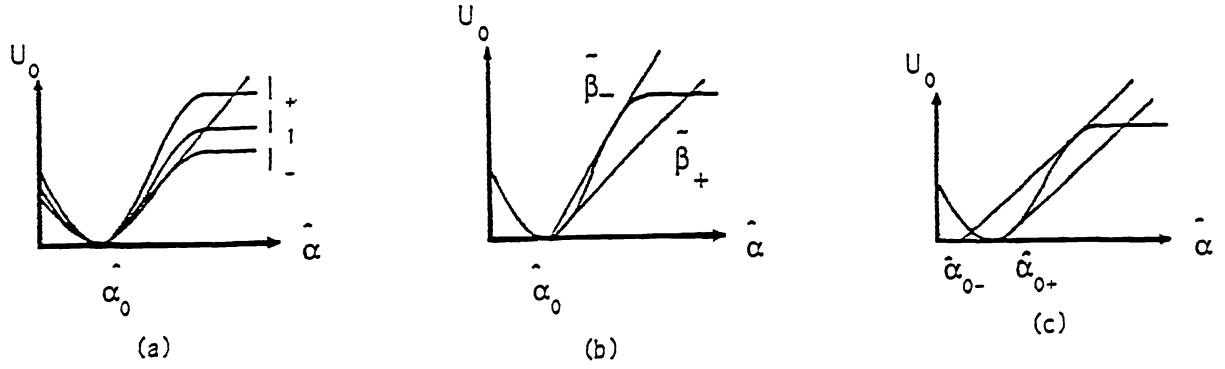

Fig. 3. Three modes of operation of the acousto-optic bistable device (after[1]): (a) input intensity tuning, (b) feedback gain tuning, (c) bias voltage tuning.

Fig. 3(a) shows the mode of operation leading to hysteretic behavior in the output versus input intensity curve. The straight line starting from $\hat{\alpha} = \hat{\alpha}_0$ corresponds to the feedback loop. Changing the laser intensity from lower bistability limit I_- to upper bistability limit I_+ one gets all the intermediate curves between I_- and I_+. Let the curve marked I_1 correspond to the initial laser intensity (I_1). The operating point $\hat{\alpha}_0$ is chosen in such a way that the feedback line crosses the curve I_1 both in the lower part of the curve, i.e., the "off" state, from initial off state to on state, one has to increase the input laser intensity from I_1 to I_+, for which only one solution of formulations (1a) and (5) exists. When the input intensity is decreased, the system still stays in the on state until the feedback line is tangent to the transmission curve marked I_-, where the system switches to the off state.

Fig. 3(b) describes the feedback tuning mode with the input intensity fixed. It is possible to switch from off to on and vice versa by changing β, where β is the inverse of the slope of the feedback line. The parameters β_+ and β_- are the maximum and minimum gains for bistability, respectively.

Fig. 3(c) shows the third mode of operation for a varying bias voltage $\hat{\alpha}_0$ with the input intensity and gain fixed. The values $\hat{\alpha}_{0-}$ and $\hat{\alpha}_{0+}$ are the voltage limits within which bistability is obtained.

Under the feedback condition, $\hat{\alpha}$ can be treated as a constant during the interaction if and only if the interaction time is much smaller compared with the feedback delays involving the response time of the photodetector, the sound cell driver, the feedback amplifier, and any variable delay in the feedback path. Banerjee and Poon [7] considered this delay-based feedback mechanism and used FORTRAN programming to simulate the action of the device in the Bragg regime. With a fixed $\hat{\alpha}_0$ the output E_1 will undergo a series of interactions at every instant $\hat{\alpha}$ is updated through the feedback action. Using eqs.(3a) and (5), E_1 after n iterations can be written as

$$E_1(n+1) = E_{Inc} \sin\left[\frac{\hat{\alpha}_0 + \beta E_1^{\,2}(n)}{2}\right] \quad . \tag{6}$$

The analysis of Eq. (6) involves theory of dynamical systems [9,10] for quadratic maps of the type

$$X_{n+1} = \mu X_n (1 - X_n) \quad , \tag{7}$$

where μ is a parameter. The behavior of eq.(7) is simple dynamically for $0 \le \mu \le 3$ and chaotic for $\mu \ge 4$. Chrostowski [3] has analyzed the bifurcation in acousto-optic bistability in a single input device using nonlinear dynamical analysis. In his work, the behavior of eq.(6) is essential for considering the light intensity $|E_1|^2$ represented via the quadratic map

$$X_{n+1} = 1 - \lambda \sin^2 (X_n - 0.5) \quad , \tag{8}$$

which maps the interval $0 \le X \le 1$ into the interval $(1 - \lambda) \le X \le 1$. A deterministic map of this equation is given by Fig. 4.

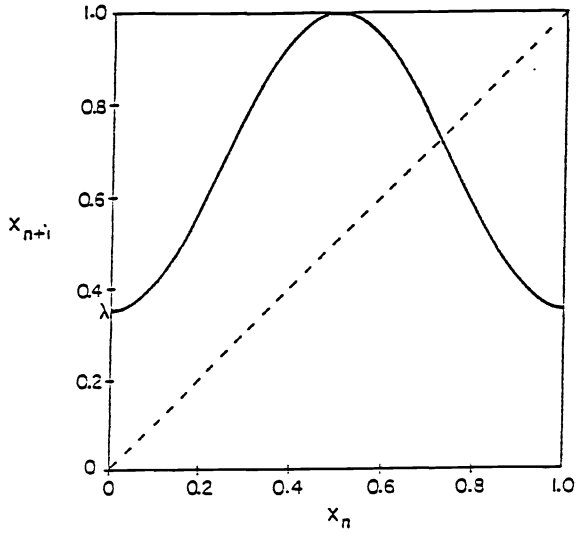

Fig. 4. Deterministic map $X_{n+1}=1-\lambda\sin^2\pi(X_n-0.5)$ (after [3]).

Here X_n and X_{n+1} are the inputs to the acousto-optic driver (rf modulator) at different times, λ ($=I_L G k \beta$) is the bifurcation parameter, I_L is the input laser intensity, G is a geometric factor, k is the light-voltage conversion ratio of the photodetector, and β is the feedback amplifier gain. The first bifurcation occurs around $\lambda=0.32$, generating two states, and a second bifurcation occurs around $\lambda=0.63$ generating multiple states. For bistable operation the range $0.32<\lambda<0.63$ is chosen.

Chatterjee *et al.* [6] applied this analysis to the zeroth order optical flip-flop (discussed later in the section IV). For notational consistency, the connections between the symbols in Chrostowski and Chatterjee *et al.* are shown in Table 1.

Table 1. Relations between the symbols in Chrostowski [3[and Chatterjee *et al.* [6]

Chrostowski	Chatterjee *et al.*
X_n	$\hat{\alpha}_n/2\pi$
λ	$\beta E_{inc}^2/2\pi$, $1-\hat{\alpha}_0/2\pi$
β	$\beta/2\pi Gk$

For the zeroth-order optical flip-flop $\hat{\alpha}_0$ is set to zero. The system equation may be written as

$$\hat{\alpha}_{n+1} = f(\hat{\alpha}_n) = \beta E_{inc}{}^2 \sin^2 \frac{\hat{\alpha}_n}{2} \quad , \tag{9}$$

where $\hat{\alpha}_n$ and $\hat{\alpha}_{n+1}$ the inputs to the acoustic driver at different times.

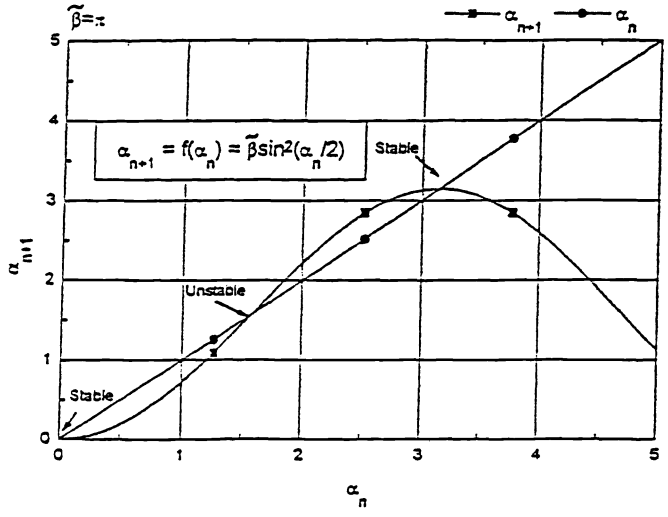

Fig. 5. Deterministic map of the zeroth-order optical flip-flop (after [6]).

Considering for simplicity E_{inc} as equal to one, a deterministic map for this equation can be generated, such as the one shown in Fig. 5 for $\beta=\pi$. As shown in the figure, there are three intersection points, of which the two outer points are stable, while that in the center is unstable. As the amplitude of $f(\hat{\alpha}_n)$ is now proportional to β, it can be shown that for $\beta < 0.9\pi$ it falls below the unit straight line. In this case there is no intersection between $f(\hat{\alpha}_n)$ and $\hat{\alpha}_{n+1}$, except at the origin. The system is monostable.

Fig. 6a shows this case for $\beta=0.6\pi$. When β is increased beyond 0.9π (Fig. 6(b)) to π, there are two points of convergence: π (for $\hat{\alpha}_n>1.57$) and 0 (for $\hat{\alpha}_n<1.57$). This value of β corresponds to a bistable system. As β is more increased to $\beta=4.0$, as shown in Fig. 6(c), the system has three stable points: two self looping at 3.4 and 4.0 (for $\hat{\alpha}_n>1.13$), and the third at 0 ($\hat{\alpha}_n<1.13$). These oscillations represent a bifurcation. When β is increased to 1.7π (Fig. (6d)) the system is in chaos.

The action of the acousto-optic device with feedback can also be simulated on a personal computer via FORTRAN programming, or SPICE modeling, as already discussed. The concept of using an equivalent electrical circuit model to represent the A-O hybrid dynamical system, it appears, was first anticipated by Chrostowski *et al.* [4] in 1983. This model, which incorporates dependent sources, delay lines, and first order RC stages, is a precursor to the nonlinear SPICE model used independently later by Chatterjee and Huang [5]. The latter approach will be presented in greater detail in the following section. If the diffracted electric field E_1 is plotted as a function of $\hat{\alpha}_0$, with β as a parameter, bistability, hysteresis and chaos can be demonstrated. Considering $\hat{\alpha}_0$ as fixed, the iterated behavior of E_1 can be observed for different values of β. This yields the so-called steady-state response of the system [7]. A type of transient response results if the input $\hat{\alpha}_0$ is incremented every time the feedback comes into the summer. The input is changed in steps.

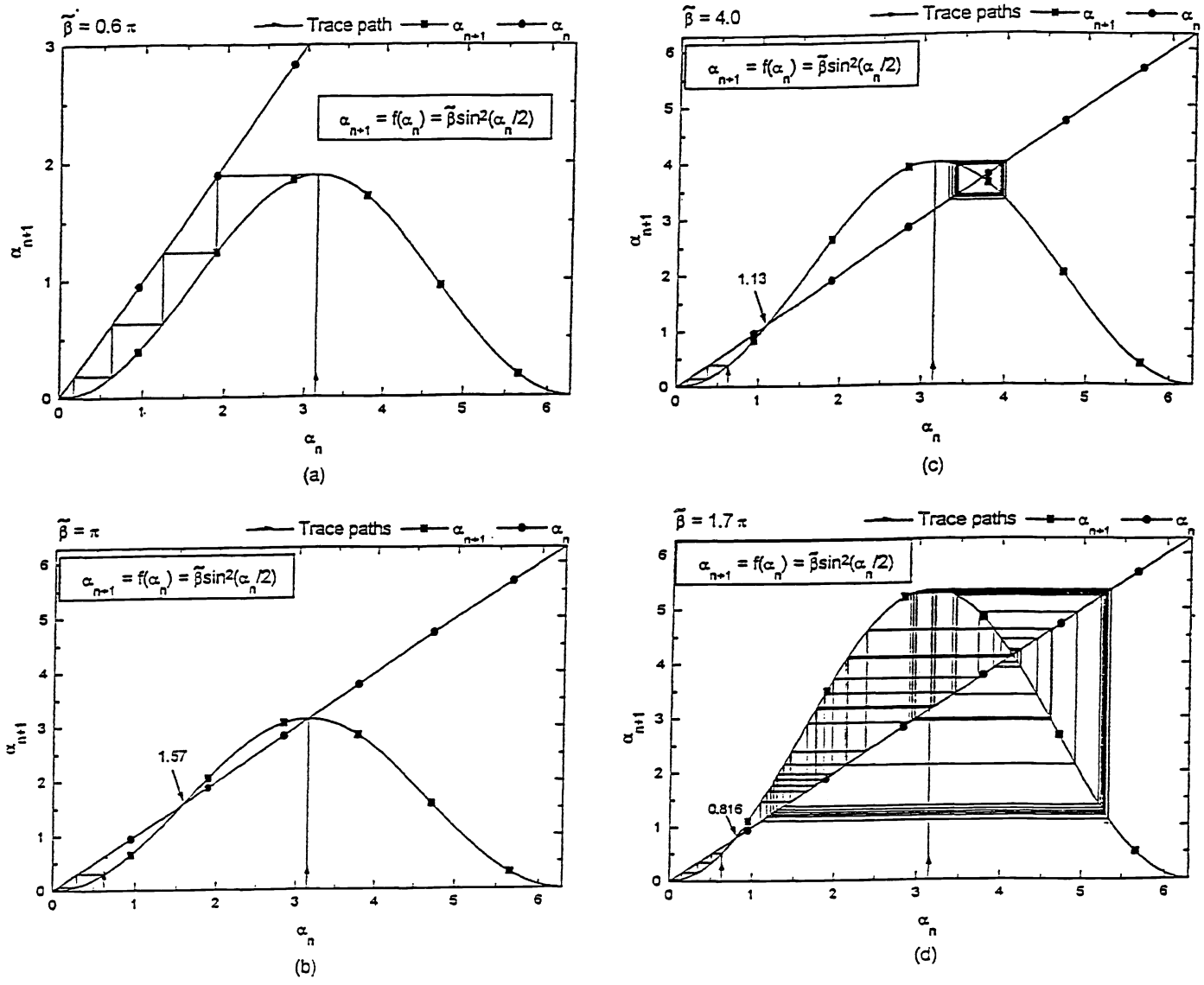

Fig. 6. Trace diagrams for several different cases (after [6]): (a) $\beta=0.6\pi$ (monostable), (b) $\beta=\pi$ (bistable), (c) $\beta=4.0$ (bifurcation), and (d) $\beta=1.7\pi$.(multistable, chaotic).

With the average rate of change being given by the ratio of the increment $\Delta\hat{\alpha}$ and the delay in the feedback. This change in $\hat{\alpha}$ is related to an equivalent feedback delay (t_d) through the following relationship,

$$t_d = \left(\frac{\Delta\hat{\alpha}_0}{2\hat{\alpha}_{0p}} \right) t_{\hat{\alpha}} \tag{10}$$

where t_α is the total sweep time of the input and $\hat{\alpha}_{0p}$ is the peak value of $\hat{\alpha}_0$. Note that the $\hat{\alpha}$ increment ($\Delta\hat{\alpha}$) in Eq. (8), which contributes to the feedback delay, is similar to the corresponding parameter in ref.[5]. Likewise, the delay t_d mentioned here reappears in the SPICE-based work by Chatterjee and co-workers [5,6]. If the delay is ignored, the point where the slope of the E_1 versus $\hat{\alpha}_0$ curve becomes zero is at

$$\hat{\alpha}_{0(sat)} = \pi - \beta \tag{11}$$

In Banerjee and Poon [7], however, the time delay is not discussed explicitly.

3. THE HYBRID A-O DEVICE: SPICE MODELING

In this section we discuss nonlinear modeling of the hybrid A-O device. Each physical system can be modeled using a circuit model. In many cases circuit models are simpler to understand and easier to test than other models. After developing a reasonably good circuit model, it becomes considerably more convenient to investigate the characteristics of the hybrid device by means of the model. A circuit model that is appropriate for simulation that uses I-G SPICE package has been developed by Chatterjee *et al.* [5,6]. Three types of equivalent circuit models are used to demonstrate optical bistability, multistability, and chaos in these simulations.

Considering the interaction time in the device to be much smaller than the delay in the feedback path, $\hat{\alpha}$ can be treated as constant during the interaction. Combining the eqs.(1a) and (5) at ξ=1 (output of the acousto-optic device) we have

$$E_1\Big|_{\xi=1} = E_{inc} \sin\left(\frac{\hat{\alpha}_0}{2} + \frac{\beta}{2} E_1^{\,2} \right) \tag{12}$$

This equation specifies the nature of the evolution of E_1 at the output. Because it was impossible to represent eq.(12) entirely by a nonlinear SPICE model at that time, it is expanded in an infinite Taylor series

$$E_1 = E_{inc}\left[\left(\frac{\hat{\alpha}_0}{2} + \frac{\beta}{2} E_1^{\,2} \right) - \frac{1}{3!}\left(\frac{\hat{\alpha}_0}{2} + \frac{\beta}{2} E_1^{\,2} \right)^3 \quad + \frac{1}{5!}\left(\frac{\hat{\alpha}_0}{2} + \frac{\beta}{2} E_1^{\,2} \right)^5 - \frac{1}{7!}\left(\frac{\hat{\alpha}_0}{2} + \frac{\beta}{2} E_1^{\,2} \right)^7 \right] + \ldots \tag{13}$$

This series is truncated after a certain order (which is 17 in this case) to get an accuracy above 90%.

At this stage it is necessary to find a way to deal with the time delay in the feedback path. This goal leads to think about an element that can exhibit time delay without loading the system in circuit domain. A good choice turns out to be a lossless transmission line. This element exhibits time delay without loading the system in the circuit domain. To ensure the line is properly terminated, it is connected to a load which has the same impedance as the line i.e., characteristic impedance of the line. As a result, there is no reflected wave in the load end (Γ = 1). The transmission line delay TD represents the time delay in the feedback loop. The fields (voltages) E_1 and E_1' are expressed as

$$E_1'(t) = E_1(t - TD) \quad . \tag{14}$$

In this model $E_1'(t)$ is added in series with the input α_0 back into the modulator driver. By modifying eq. (11) the model equations can be described as

$$\hat{\alpha}$$

$$E_2[\hat{\alpha}_0(t), E_1'(t)] = \frac{1}{2}\hat{\alpha}_0(t) + \frac{\beta}{2}E_1'^2(t) = \frac{1}{2}\hat{\alpha}_0(t) + \frac{\beta}{2}E_1^2(t - TD) \tag{15}$$

$$E_1 = E_2 - \frac{1}{3!}E_2^3 + \frac{1}{5!}E_2^5 - \frac{1}{7!}E_2^7 + \ldots + \frac{1}{17!}E_2^{17} \tag{16}$$

These equations result in a model that simulates the bistable acousto-optic device adequately. It clearly illustrates the property of the feedback time delay. Simulations give similar results as those obtained by other methods [1,3,7,8]. A special feature of this model is that time delay can be adjusted to investigate its effect on the hybrid device. Although in new versions of SPICE nonlinearities can be introduced, the results are basically the same. Three types of models are shown in Fig. 7. These models are used to exhibit the effects of bias, feedback gain, and input amplitude on the output of the hybrid device.

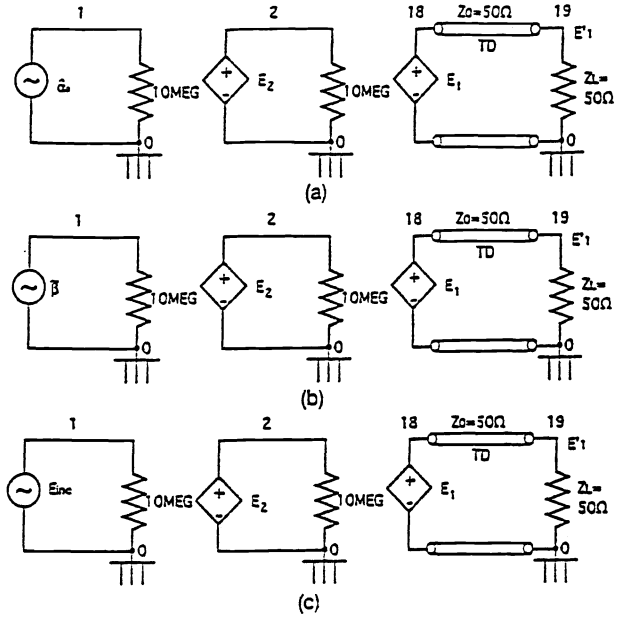

Fig. 7. (a) Circuit model using dependent voltage source and a lossless transmission line to exhibit the time delay in the feedback loop of the acousto-optic device. (b) A feedback-gain tuning circuit model (c) An input amplitude tuning circuit model (after [5]).

Now we look to the simulations of these three different models. First we consider the model for bias voltage tuning given in Fig. (7a). Here $\hat{\alpha}_0$ is a triangle input; the input amplitude E_{inc} is set to 1 for convenience.

Fig. 8 is an intensity versus a symmetric triangular input bias duration graph corresponding to the first-order light. Although the input bias is symmetric, the output intensity is not. This causes the hysteresis loops we get in Fig. 8 which is an intensity versus bias voltage graph for both first-order and zeroth-order lights. The critical requirement for the formation of a hysteresis loop is the presence of a finite time delay in the feedback path of the system. Without the delay a bistable curve has no memory and zero loop area occurs. This simulation is similar to the experimental result that is shown in Fig. 9(b). Chrostowski *et al.* [1] obtained this experimental (input intensity and the gain being kept fixed) curve for bias voltage tuning mode of the acousto-optic bistable device.

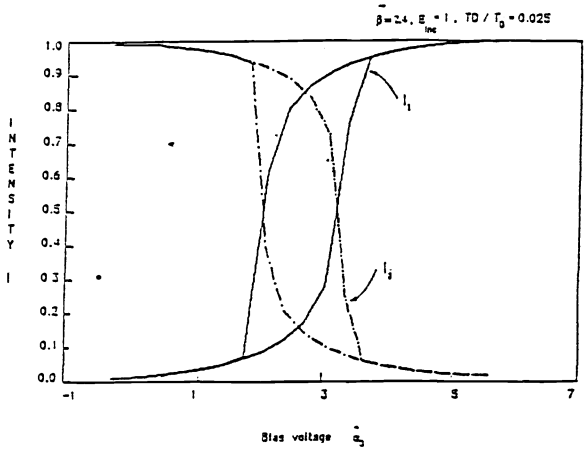

Fig. 8. Superposed graphs of I_0 and I_1, indicating conservation of diffracted energy (after [5]).

Fig. 9(a). Bias voltage bistability (after [1]).

If the feedback time delay is changed with fixed feedback gain in these simulations, it is seen that the area under the hysteresis increases for larger time delays. The right edge of the loop moves to the left. For a large time delay the system is slow in attaining saturation, as well as in returning to its low (or high) value. If the feedback gain is changed keeping the other variables constant, for increasing gain the hysteresis loop moves to the left. Simulation results are shown for various time delays in Fig. 9(b) and for various feedback gains in Fig. 9(c).

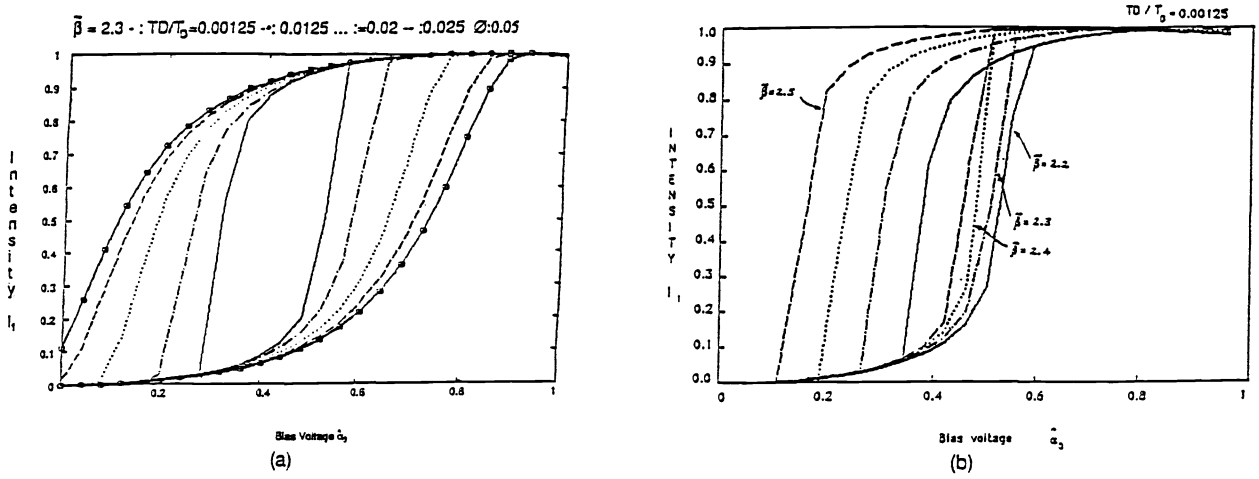

Fig.9. Change of hysteresis loop width for (b) varying time delays and (c) varying feedback gains (after [5]).

In Fig. 10(a) and 10(b) bias voltage $\hat{\alpha}_0$ is changed from –0.7 to 2π. Emergence of double loops is observed with the particular choice of parameters. The system exhibits possible multistable behavior by an increasing time delay (Fig. 10(a)). When the time delay is increased more it enters multiple oscillations (Fig. 10(b)).

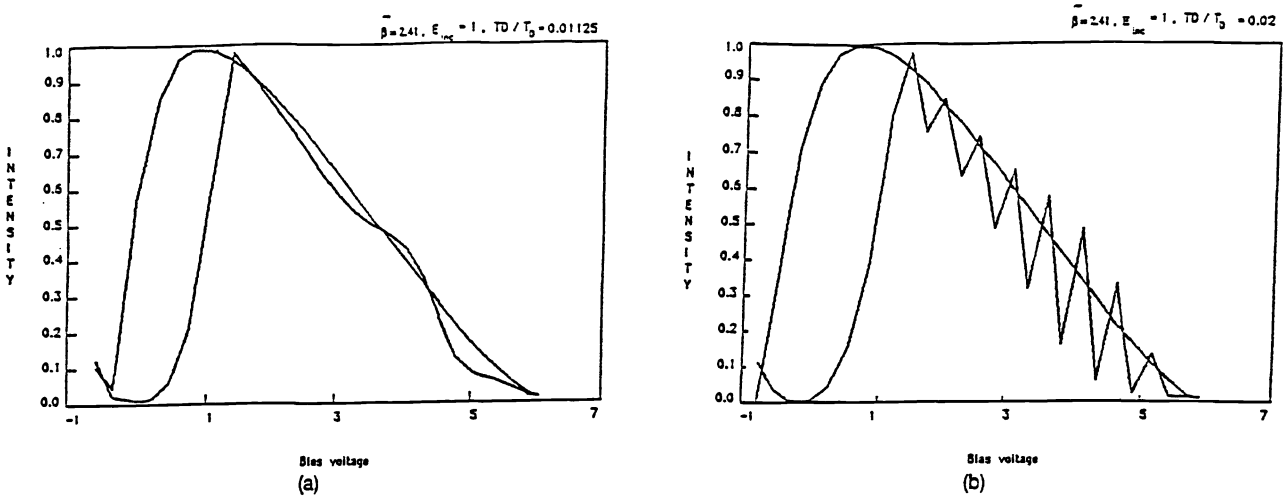

Fig. 10. Intensity I_1 versus bias voltage (α), showing (a) emergence of three additional loops for a higher time delay time and (b) illustration of multiple oscillation beyond saturation point for a time delay (after [5]).

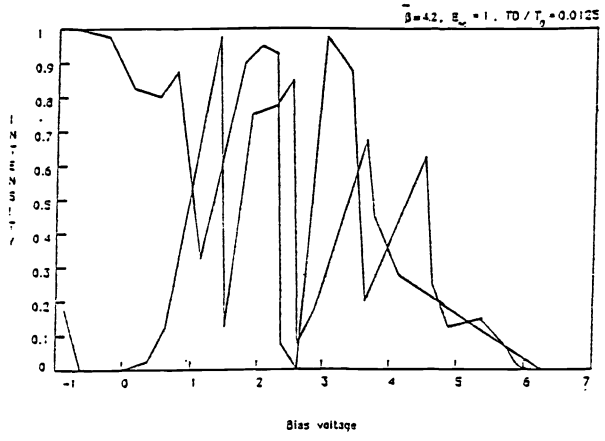

Fig. 11. Intensity I_1 for feedback gain tuning β, showing regular hysteresis (after [5]).

When feedback gain β is also increased the system becomes extremely oscillatory, essentially enters into chaos as shown in Fig. 11. Another interesting aspect of chaos is manifested for the case of bias voltage tuning under an I_0-type feedback. In this case, since the feedback consists of a cosine function instead of a sine, it turns out that for a specific "large" value of β and the time delay, chaotic oscillations occur both to the right and to the left of the primary hysteresis loop. This result, shown under SPICE simulation in Fig. 12(a) is expected if one follows the iteration map shown in Fig. 12(b).

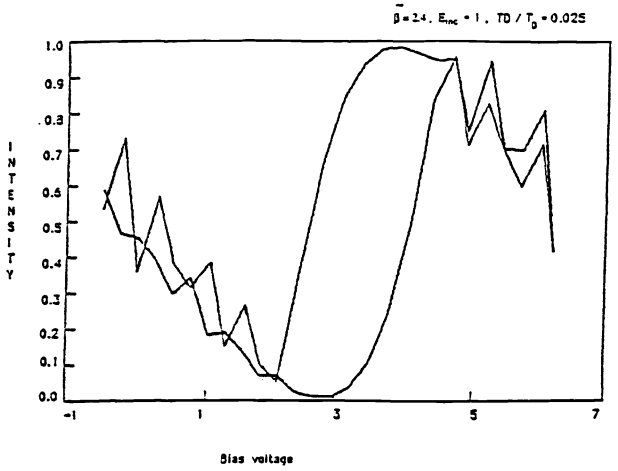

Fig. 12(a). Intensity I_1 versus bias voltage (α_0) showing illustration of multiple oscillation beyond saturation point for a high time delay (after [5]).

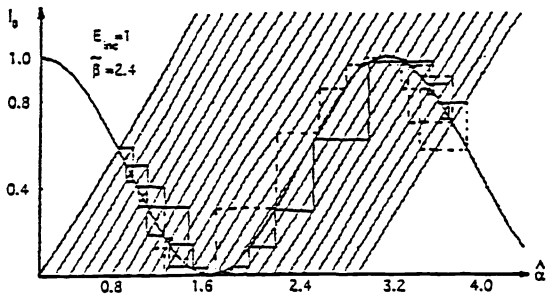

Fig. 12(b). Depiction of orbit for parameters (after [5]).

4. HYBRID A-O S-R FLIP-FLOP

Thus far, we have reviewed various studies on the dynamical and hysteretic behavior of hybrid acousto-optic bistable device. Chatterjee *et al.* [6] have shown that a dual input hybrid acousto-optic bistable device functions as a set-reset flip-flop. To this end, we consider a Bragg cell on which two input light beams are incident symmetrically. Let the two beams of amplitudes E_{inc0} and E_{inc1} be incident at negative and positive Bragg angles, respectively, as shown in Fig. 13.

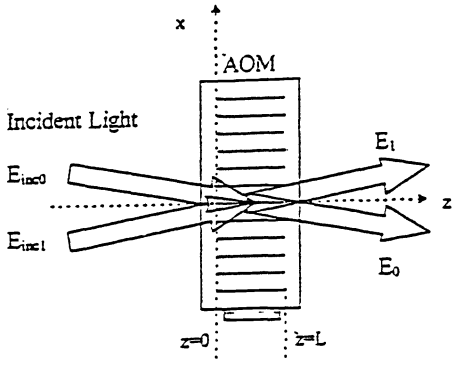

Fig.13. Dual-input acousto-optic cell, with the two beams incident symmetrically relative to the horizantal axis at θ_B , the Bragg angle (after [6]).

To determine the diffracted outputs, the well-known coupled differential equations [11] for the two Bragg orders (eqs.1(a,b)) with the boundary conditions

$$E_0(z=0) = E_{inc0},$$
$$E_1(z=0) = E_{inc1}, \tag{17}$$

for the E fields at z=0 must be solved. The solutions may be obtained as

$$E_0 = E_{inc0}\cos\left(\frac{\hat{\alpha}}{2}\xi\right) - jE_{inc1}\sin\left(\frac{\hat{\alpha}}{2}\xi\right),$$
$$E_1 = E_{inc1}\cos\left(\frac{\hat{\alpha}}{2}\xi\right) - jE_{inc0}\sin\left(\frac{\hat{\alpha}}{2}\xi\right). \tag{18}$$

These equations can be expressed in intensity form as

$$I_0 = I_{inc0}\cos^2\left(\frac{\hat{\alpha}}{2}\xi\right) + I_{inc1}\sin^2\left(\frac{\hat{\alpha}}{2}\xi\right),$$
$$I_1 = I_{inc1}\cos^2\left(\frac{\hat{\alpha}}{2}\xi\right) + I_{inc0}\sin^2\left(\frac{\hat{\alpha}}{2}\xi\right). \tag{19}$$

where $I_{inc0}=E_{inc0}^2$, $I_{inc1}=E_{inc1}^2$. We note from above solutions that switching of the two beams occurs when $\hat{\alpha}=\pi$ and $\xi=1$. Fig. 13 shows this switching effect observed at z=L. At z=0, the intensities I_0 and I_1 have been normalized to 1.0 and 0.25 respectively. When $\hat{\alpha}=0$, no sound wave is applied; hence, the output intensities remain unchanged. When $\hat{\alpha}$ changes from 0 to π, the two beams exchange their energies.

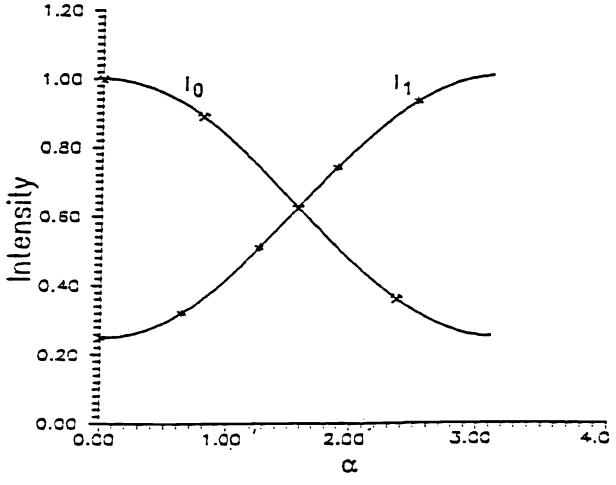

Fig. 14. Energy exchange between coupled orders (after [5]).

This switching property combined with a feedback mechanism results in a set-reset flip-flop. There are two possible configurations, viz, a zeroth-order or a first-order, depending on which order output is used for the feedback mechanism.

Fig. 15 shows the zeroth-order acousto-optic flip-flop. The zeroth-order E_0 at the output is detected and fed back through a time delay element and an effective feedback path gain β to the acoustic driver. The open-loop bias to the acoustic driver, represented by $\hat{\alpha}_0$, is combined with the feedback signal to produce the equivalent bias for the acoustic driver. The input $\hat{\alpha}$ to the acoustic driver is given as

$$\hat{\alpha} = \hat{\alpha}_0 + \beta\, I_0(t - TD) \quad = \hat{\alpha}_0 + \beta \left\{ {E_{inc0}}^2 \cos^2\left[\frac{\hat{\alpha}(t-TD)}{2}\right] + {E_{inc1}}^2 \sin^2\left[\frac{\hat{\alpha}(t-TD)}{2}\right] \right\} \tag{20}$$

where TD is the time delay in the feedback loop and I_0 is the zeroth-order light intensity.

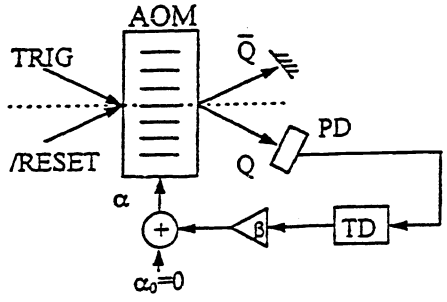

Fig.15. Schematic of zeroth-order S-R flip-flop (after [6]).

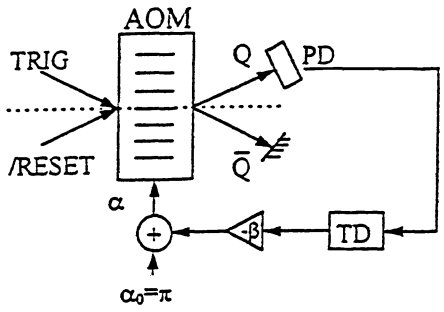

Fig.16. Schematic of first-order S-R flip-flop (after [6]).

If $\hat{\alpha}_0$ is adjusted to π and the diffracted output E_1 is taken as the source of a negative feedback, as shown in Fig. 16, then we have a first-order flip-flop.

As discussed in section III, the acousto optic bistable device can be modeled by use of equivalent non-linear circuit models and simulated with commonly available circuit-simulation software. In Fig. 17 we show the SPICE circuit model of a dual-input zeroth-order bistable device [6]. The acousto-optic modulator is modeled with sine and cosine functions by means of nonlinear dependent sources with Taylor series expansions.

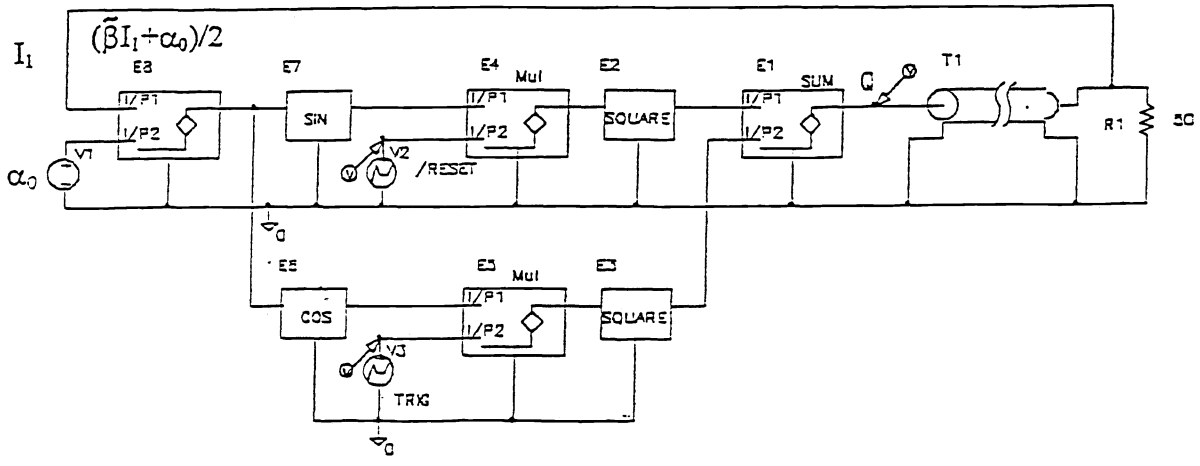

Fig. 17. SPICE-based schematic of a hybrid acousto-optic S-R flip-flop (after [6]).

The circuit time-delay element is represented by a transmission line T_1 with proper termination, and the photodetector is squaring-operator element that uses another nonlinear dependent source.

Fig. 18 shows the simulation result for a zeroth-order acousto-optic flip-flop. The /RESET is set to 1 and the TRIG is 0 in the beginning. An impulse is applied as the TRIG signal at 2 ms. The output rises with a slope and maintains a level at approximately 1. At 6 ms, the /RESET is applied with a negative impulse and is then forced to 0 during the pulse. The output returns to zero because of the consequent removal of the feedback caused by the negative impulse.

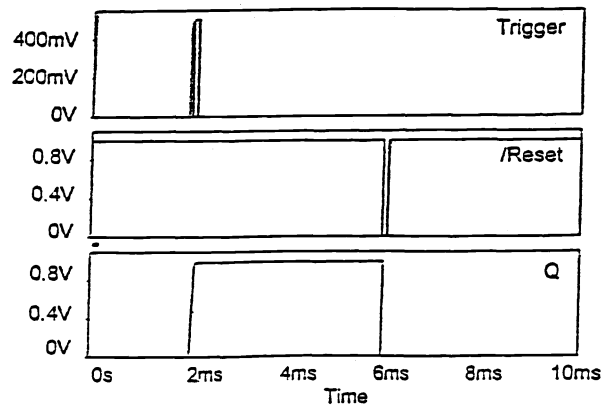

Fig.18. SPICE output for a zeroth-order flip-flop (after [6]).

It is also found that the device undergoes bifurcation and exhibits chaotic behavior when the gain β exceeds 4.0. Bifurcation and chaotic oscillations are shown in Figs. 19(a) and (b). Simulation for the first-order acousto-optic flip-flop may similarly be carried out.

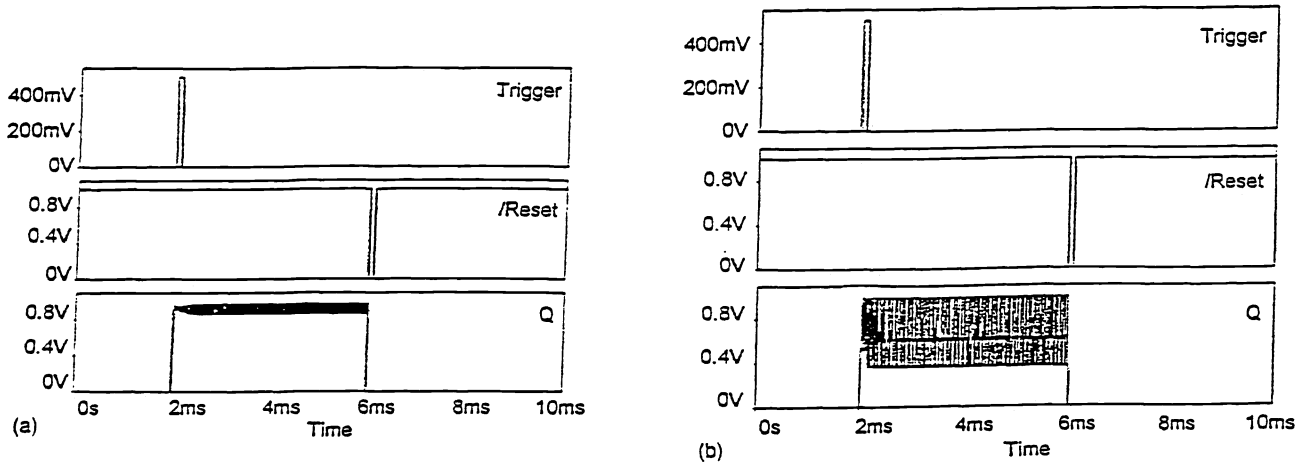

Fig.19. (a) Bifurcation and (b) chaotic oscillations in an experimental zeroth-order S-R flip-flop (after [6]).

An experimental setup for a zeroth-order acousto-optic flip-flop is also shown in Fig. 20 [6].

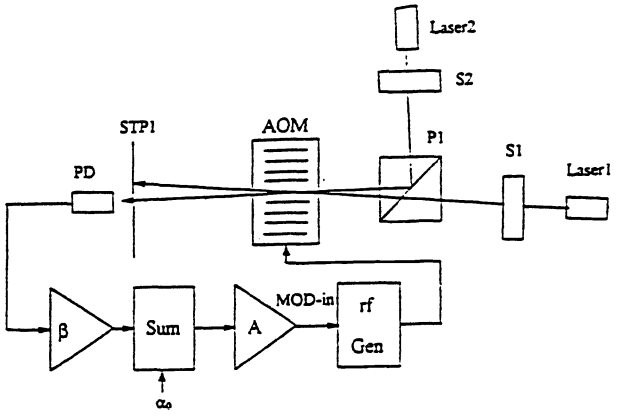

Fig.20. Experimental setup for a zeroth-order A-O S-R flip-flop (after [6]).

5. DEVELOPMENT OF DISCRETE LOGIC DEVICES

As a follow-up to the set-reset flip-flop using a two-input acousto-optic hybrid device, more recent effort has concentrated on the development of optical logic devices based on the Bragg cell, and actual logical applications to digital computations. In some recent investigations, devices based on the basic Bragg cell with proper modifications have been shown to realize an inverter, AND gate, and an OR gate, with a sensing mechanism applied to the incoming light. As these gates don't have a memory, we do not need a feedback mechanism to realize such Bragg cell-based logic gates.

To realize an inverter a bias light beam is incident at the negative (upshifted) Bragg angle. The incoming (signal) light beam is directed to a light detector that sends a signal to a device which internally generates the necessary sound driver amplitude corresponding to an effective phase delay α for the Bragg cell that ensures the required output state. To realize AND / OR gates, a similar technique may be employed. For these gates, two light beams are incident at negative and positive Bragg angles, of which the one at positive Bragg angle goes directly into the Bragg cell whereas a small amount of the light beam incident at negative Bragg angle is transferred to a light detector via a partially reflecting mirror. As was described for the inverter operation, the light detector in this case once again sends a signal to a device which internally generates the necessary sound driver amplitude corresponding to an effective phase delay α for the Bragg cell that ensures the required output state. The truth tables indicating inverter, AND and OR gates, and the necessary effective α values are listed in Tables 2, 3 and 4.

Table 2. Inverter truth table with corresponding α levels

I_{inc}	Bragg Cell Input	Bragg Cell Output	α
0 (L)	1(H)	1 (H)	0
1 (H)	1 (H)	0 (L)	π

Tables 3 and 4. AND/OR truth tables with corresponding α levels

I_{inc0}	I_{inc1}	Output	α
0(L)	0(L)	0 (L)	×
0(L)	1(H)	0(L)	0
1(H)	0(L)	0(L)	π
1(H)	1(H)	1(H)	×

I_{inc0}	I_{inc1}	Output	α
0(L)	0(L)	0 (L)	×
0(L)	1(H)	0(H)	π
1(H)	0(L)	0(H)	0
1(H)	1(H)	1(H)	×

Schematic diagrams for an inverter and that for an AND/OR gate using Bragg cells are shown in Fig. 21.

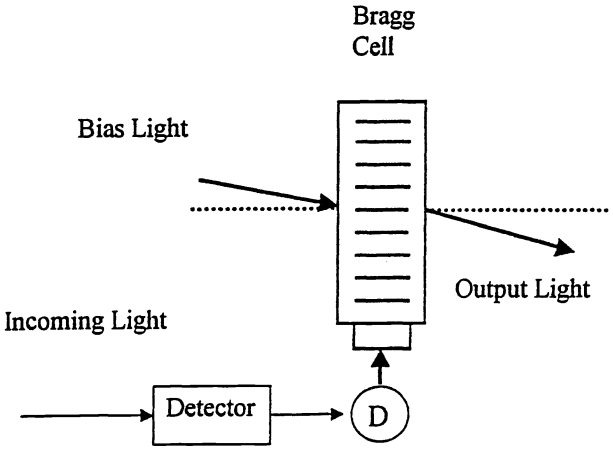

Fig. 21(a). Schematic arrangement for A-O inverter.

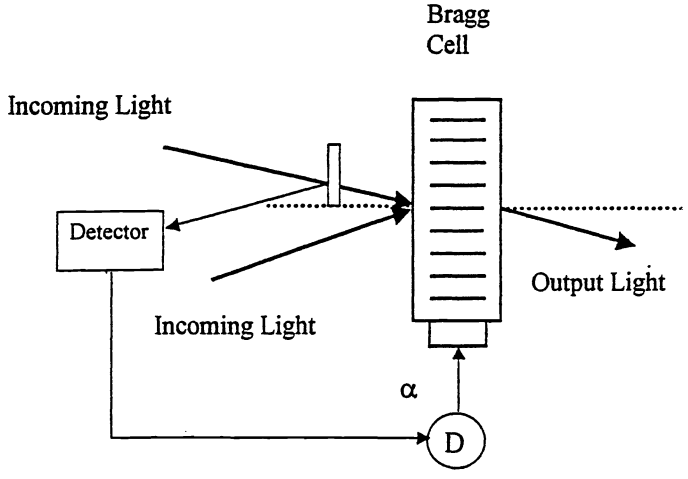

Fig. 21(b). Schematic arrangement for A-O AND/OR gates.

The above devices may be modeled using PSPICE. A PSPICE circuit model for an inverter is shown in Fig. 22. The acousto-optic modulator output intensity is modeled in this case as a cosine-squared function since the output state being monitored for inverter operation is the zeroth order. The input light intensity is represented as a voltage source I_{in} that changes between 0 and 1V. An opamp and a limiter are used to set the phase delay α of the Bragg cell to either zero or pi in order to make output light intensity free of transitional ripples due to finite input rise and fall times. The opamp is configured as a comparator whose reference is set at the 50% of the separation between the logical low and high states. In this case, we set the reference to 0.5V; this procedure ensures that α drops to zero when I_{in} drops below the reference voltage, and to pi when I_{in} rises above the reference voltage.

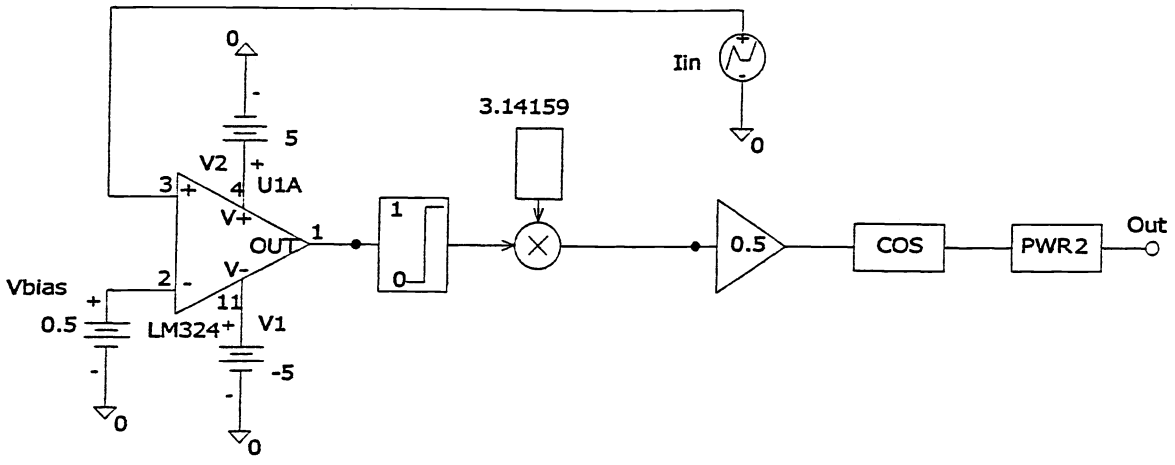

Fig. 22. Equivalent circuit diagram of an A-O inverter.

The simulation is carried out by use of the PSPICE circuit simulation program. Fig. 23(a) shows a piecewise linear input intensity and Fig. 23 (b) the corresponding output intensity waveform. The input intensity is set to 1V in the beginning. The output is zero at that time. At 3 ms the input begins to fall towards zero. When it falls to 0.5V, the output changes instantaneously to 1V, as expected. The output remains at 1V between 3.5ms and 4ms as long as the input is at 0 or, if rising, stays below 0.5V. During the rise cycle, the output goes back to zero as soon as the input surpasses the 0.5V reference.

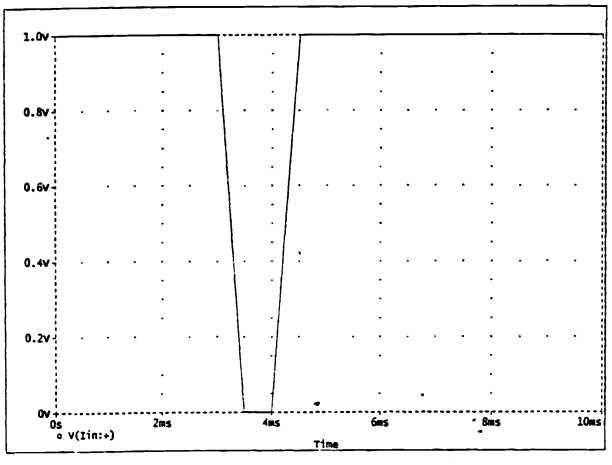

Fig. 23(a). Inverter input intensity waveform.

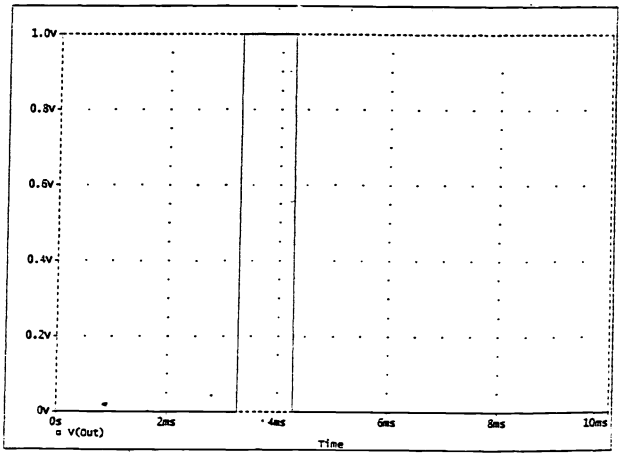

Fig. 23(b). Inverter output intensity waveform.

The SPICE model for the AND gate is shown in Fig. 24. In this model, the output logic state is chosen to be the zeroth order, whose intensity is determined by eq.(19). In accordance with this equation, we realize the AND output conditions by setting one of the input beams to either a logical zero or one (for simulation purposes only; in the real Bragg cell, of course, this input is also allowed to make finite-slope transitions); the other input beam is partially detected, and the feed-forward network sets the desired α value to either zero or pi, corresponding to the 50% threshold setting as was used for the A-O inverter. In this case, however, there is a small difference in the nature of the output logical states. Since the output intensity

has contributions from both inputs, even when the α is set to zero, for instance, while the I_{inc1} contribution drops to zero, the contribution due to I_{inc0} is actually maximized; therefore, during the time that the input (I_{inc0}) crosses the 50% threshold, and approaches zero, the output level does not immediately go to zero. The converse is also true for rising I_{inc0} in that the output will not instantaneously jump to one, but go through the transition. For such a gate, therefore, the output logical state may be considered "1" whenever the output intensity is above the 50% threshold, and "0" when it is below the 50% threshold.

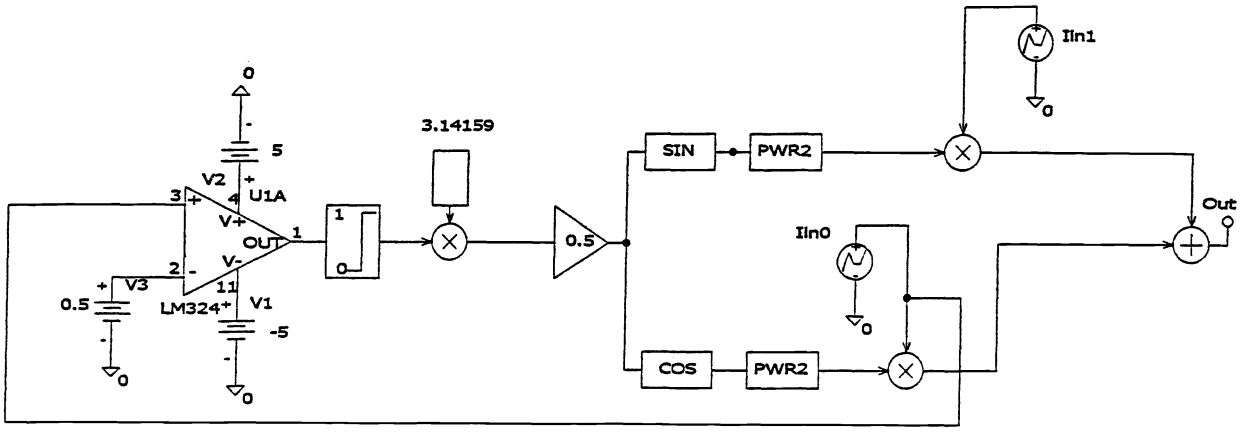

Fig. 24. Equivalent circuit diagram of an A-O AND gate.

The intensity waveforms for the AND gate inputs and the output are shown in Fig. 25. The corresponding logical states achieved at the output for the different pairs of input states can be seen to satisfy the AND operation. The slight transitional slopes in the output waveform in the neighborhood of the input transitions can be readily explained by recognizing both the 50% threshold criterion, as well as the consequence of the absolute input levels impacting the output via eq.(19). Finally, a few words about the implementation of an A-O OR gate are in order here. It turns out that the OR operation may be realized in a manner similar to that used for the AND gate. Note from the logic tables shown earlier that the A-O AND can be readily converted to an OR simply by switching the values of the feed-forward α parameter. The corresponding PSPICE simulation has been carried out; the results are not presented here.

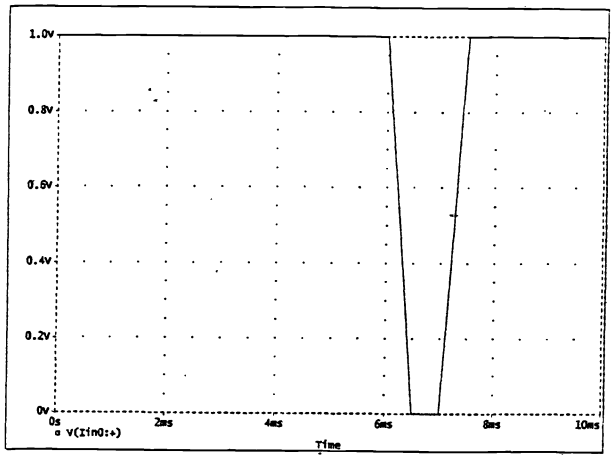

(a)

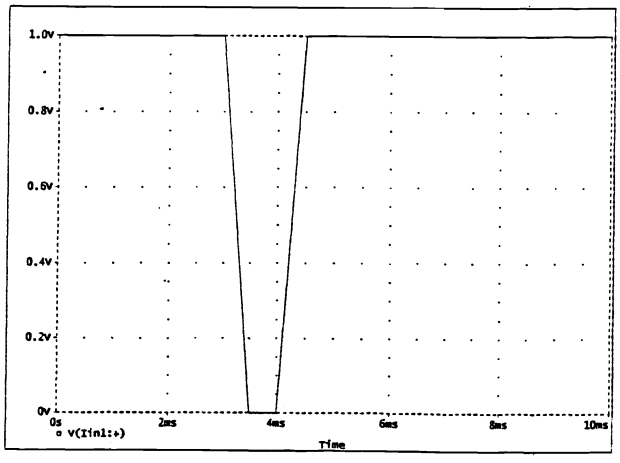

(b)

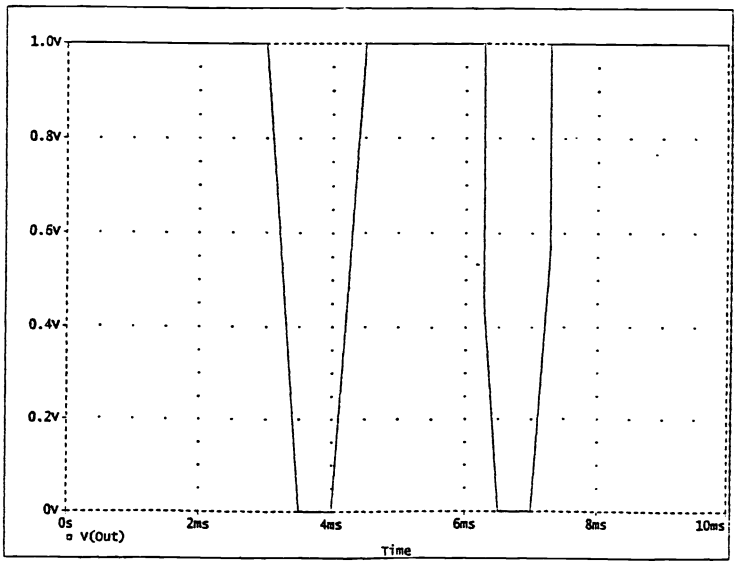

(c)

Fig. 25. (a) and (b) input intensity, and (c) output intensity waveforms.

5. CONCLUDING REMARKS

It has been shown that a basic acousto-optic Bragg cell exhibits interesting bistable and chaotic characteristics that can lead to parametric hysteresis and memory. These properties have been explored in the research literature via analytical (such as quadratic maps) methods, as well as simulations, including direct programming of the system equations under feedback delay, and the application of suitable electrical circuit models based on SPICE. It has also been shown that the bistable device may be used to develop an acousto-optic S-R flip-flop working both in zeroth- and first-order. Development of simple A-O logical devices and their PSPICE implementation has also been discussed in some detail.

6. ACKNOWLEDGMENT

This work was supported in part by a grant from the National Science Foundation under grant number EEC-9980281.

7. REFERENCES

1. J. Chrostrowski and C. Delisle, "Bistable optical switching based on Bragg diffraction," *Opt. Commun.*, pp. 71-74, 1982.
2 J. Chrostrowski, R.Vallee, and C. Delisle, "Self–pulsing and chaos in acoustooptic bistability," *Can. J. Phys.*, pp. 1143-1148, 1983.
3. J. Chrostowski, "Noisy bifurcations in acoustooptic bistability," *Phys.Rev.A*, pp. 3023-3025, 1982.
4. J. Chrostrowski, C. Delisle and R. Tremblay, "Oscillation in an acoustooptic bistable device," *Can. J. Phys.*, pp. 188-191, 1983.
5. M. R.Chatterjee and J. J.Huang, "Demonstration of acousto-optic bistability and chaos by direct nonlinear circuit modeling," *Appl. Opt.*, pp. 2506-2517, 1992.
6. M. R. Chatterjee and S.-T. Chen, "Dual-input hybrid acousto-optic set-reset flip-flop and its nonlinear dynamics," *Appl. Opt.*, pp. 3147-3154, 1997.
7. P. P. Banerjee and T.-C. Poon, " Simulation of bistability and chaos in hybrid devices," *Proc. of the 30th Midwest Symposium on Circuits and Systems*, K. Jabber, (Ed.), North-Holland, Amsterdam, pp. 820-823, 1987.
8. T.-C. Poon, and S.-K. Cheung, "Performance of a hybrid bistable device using an acoustooptic modulator," *Appl. Opt.*, pp. 4787-4791, 1989.
9. R.L. Devaney, *An Introduction to Chaotic Dynamical Systems* (Benjamin-Cummings, Redwood City, California, 1986).
10. J.M.T. Thompson and H.B. Stewart, *Nonlinear Dynamics and Chaos* (John Wiley & Sons, Inc., New York, 1986).
11. A. Korpel and T.-C. Poon, "Explicit formalism for acoustooptic multiple plane wave scattering," *J. Opt. Soc. Am.*, pp. 817-820, 1980.
12. M. R. Chatterjee and E. Sonmez, "Demonstration of Binary Optical Logic Devices Using Bragg Cells," Optical Society of America Annual Meeting, Providence, Rhode Island, October 2000.